

Article

LaSCA: A Visualization Analysis Tool for Microstructure of Complex Systems

Zean Tian ^{*}, Zhongyang Zhang, Xiao Jiang, Feng Wei, Shen Ping and Fan Wu

College of Computer Science and Electronic Engineering, Hunan University, Changsha 410082, China

* Correspondence: tianzean@hnu.edu.cn

Abstract: Over the past few decades, plenty of visualization software for the structural analysis of disordered/complex systems has been developed, but the uniqueness and correctness of structural quantification for such systems are still challenging. This paper introduces a visualization analysis tool based on the largest standard cluster analysis (LaSCA), which satisfies the three essential requirements for general structural analysis: physical correctness, objective identification, and injective representation. The specific functionalities of LaSCA include the directed graph model of complex systems, novel structural parameters, topologically close-packed structures, arbitrary partial pair distribution functions, the identification of long-range ordered structures, the adaptive selection of graphical elements, the tracking display of atom ID, user-defined view angles, various options for atom selection, and so on. The program is efficiently based on OpenGL hardware acceleration, employing special algorithms to treat bonds as cylinders or lines and treat atoms as spheres, icosahedrons, tetrahedrons, or points. LaSCA can process more than 1.2 million atoms within 50 s on a PC with 1 GB memory and four cores (Intel Core i7-9700). It is robust and low-cost for surveying short-, medium-, and long-range ordered structures and tracking their evolutions.

Keywords: complex system; visual analysis; LaSCA; long-range ordered structure



Citation: Tian, Z.; Zhang, Z.; Jiang, X.; Wei, F.; Ping, S.; Wu, F. LaSCA: A Visualization Analysis Tool for Microstructure of Complex Systems. *Metals* **2023**, *13*, 415. <https://doi.org/10.3390/met13020415>

Academic Editors: Varvara Romanova and Alain Pasturel

Received: 6 January 2023

Revised: 6 February 2023

Accepted: 14 February 2023

Published: 17 February 2023



Copyright: © 2023 by the authors. Licensee MDPI, Basel, Switzerland. This article is an open access article distributed under the terms and conditions of the Creative Commons Attribution (CC BY) license (<https://creativecommons.org/licenses/by/4.0/>).

1. Introduction

Computer simulation, as the third paradigm based on experimental induction and model deduction, has been widely used to quantify structures and properties of materials in recent decades [1–3]. The output of simulations and experiments is often in numerical values with spatial, time, or space–time characteristics, such as the coordinates, speeds, and energy of all atoms in a system [4]. An effective structure quantification for such systems is a prerequisite for investigating the structure–property relationship.

Many algorithms for local structure recognition have been developed in the past, falling into two categories according to whether the neighborhood of atoms depends on a preset cutoff distance R_c . An appropriate R_c is crucial for R_c -dependent methods, such as Basic Cluster Analysis [5], Common Neighbor Analysis (CNA) [6], the Honeycutt–Anderson pair (HA-pair) [7,8], and the Coordination Polyhedron Method [9]. Voronoi tessellation (VT) is an R_c -independent method that divides 2D/3D space into convex polygons/polyhedrons (around every point) without overlaps or gaps and points out that share edges (2D) or facets (3D) are neighbors with each other [10,11].

CNA is effective in recognizing local structures, such as the 13-atom FCC/HCP unit, the 15-atom BCC unit, and the 13-atom icosahedron; the dependency on R_c , however, leads to uncertainty and subjectivity in the quantification of local structures [12], deviating from the basic scientific principle of unique objectivity. Based on symmetric partition, no preset parameters are necessary to run VT; however, for disordered systems, VT may result in Voronoi Neighbor Anomaly (VNA), where some nearer neighbors are lost [13]. VNA is a serious concern when the interested object (e.g., interatomic forces and potential energy)

is sensitive to distance. In other words, when using VT to conduct structural analysis of disordered systems, physical correctness may be difficult to guarantee.

Even if the local structural characteristics of each atom have been identified, it is still very difficult to quantify various medium- and long-range structures in a complex system, such as the spacious distribution of phases in a polycrystalline system [14] and the repeat units of a topologically close-packed (TCP) crystal [15–17]. Visualization is a direct and effective means of addressing this issue. For example, Diamond is designed for crystals [18] but is unavailable for non-crystalline systems; ChemDraw [19] supports various bond types and formats, but computer science and professional chemical knowledge are prerequisites for its effective use; OVITO [20] is a cross-platform type of software, supporting bond angle analysis, CNA, and VT. Nevertheless, these types of software are either R_c -dependent or have VNA concerns. Accordingly, there is an urgent need to develop software for quantifying local structures, where unique objectivity and physical correctness are both guaranteed.

In this paper, a visualization tool called the largest standard cluster analysis (LaSCA) is represented, which is Euclidean distance-based (to avoid VNA) and R_c -independent (unique objectivity guaranteed). In Section 2, the essential requirements of general structural analysis are first summarized and then the basic logic of LaSCA, which meets all the essential requirements for general structure analysis, is clarified. Section 3 presents several specific functionalities of LaSCA. Finally, the advantages of LaSCA in identifying long-range ordered structures, visual analysis, and partial pair distribution functions (PDFs) are demonstrated through a case study.

2. Core Concepts

2.1. Basic Requirements for General Structural Analysis

A local structure is composed of a central atom and its neighbors that depart the center under a certain distance R_c . Based on this definition, a general structure analysis of atomic systems should meet three essential requirements as listed below.

Req. 1: Physical Correctness. Around an atom, all atoms in a spherical region of radius R_c should be its neighbors. In other words, there will be no situations similar to the VNA of VT.

Req. 2: Objective Identification. The identification of local structures is independent of any preset parameter. VT satisfies this requirement, while CNA, the HA-Pair, and i -CNA [9] do not.

Req. 3: Injective Representation. From local structure to representation, the symbol is injective. This requirement is not satisfied if some structures cannot be effectively labeled (e.g., HA-pair and CNA) or different structures have the same label (e.g., VT).

2.2. The Basic Logic of LaSCA

The largest standard cluster analysis (LaSCA) satisfies all the requirements mentioned above. In LaSCA, two atoms are regarded to be neighbors of each other if they depart under a certain distance r_s . In other words, the neighborhood between atoms is based on Euler distance, ensuring Req. 1.

If a pair of atoms are neighbors, a bond is used to link them; then, a local structure composed of an atom and all its neighbors can be constructed as shown in Figure 1a, in which each neighbor can comprise a reference pair (or root pair, RP) with the center. An atom shared by the two atoms of an RP is called a common near neighbor (CNN) of this RP. An RP and all its CNNs are called a common neighbor sub-cluster (CNS), as shown in Figure 1b,d. The structure feature of a CNS is represented by the connection between CNNs (see Figure 1c,e), which can be described by a CNS index ($Sijk$), where “S” is a prefix (it comes from “sub-cluster”), i stands for the total number of CNNs, j the total number of bonds between CNNs, and k the length of the longest chain composed, in part or fully, of CNNs. Thus, the CNS shown in Figure 1b is S555, and that in Figure 1d is S422.

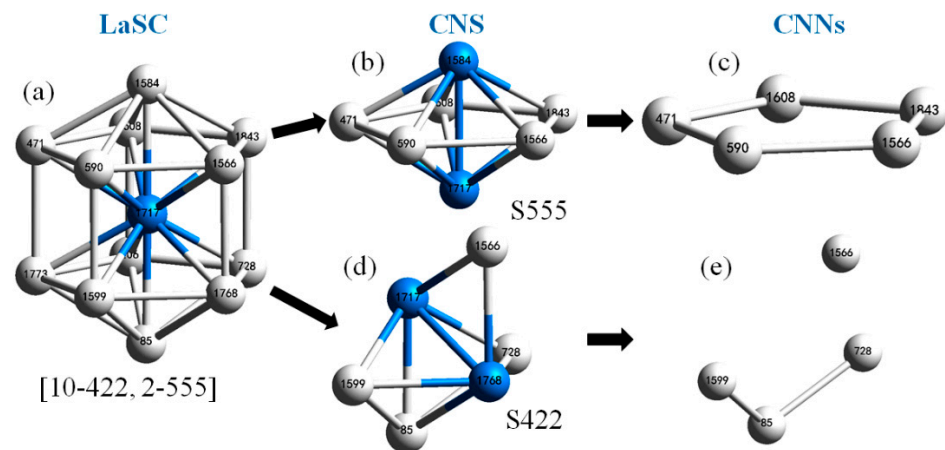


Figure 1. The logical decomposition of a largest standard cluster (LaSC). (a) Truncated decahedron (10-422, 2-555); (b) CNS S555; (c) topology of S555; (d) CNS S422; and (e) topology of S422.

The larger the value of r_s , the higher the number of neighbors around an atom and the connection between CNNs and a CNS will be more complex; when r_s is larger than some critical value, a multi-bond point (MBP, where at least three bonds meet together) and a common neighbor sub-ring (CNSR, composed partially (not entirely) of CNNs) will be inevitable. If a cluster includes neither an MBP nor a CNSR, it is defined as a standard cluster (SC). Around each atom, the largest SC (LaSC) can be uniquely identified by an algorithm [12]; meanwhile, the value of r_s for the LaSC is assigned to R_c . This identification of the LaSC not only ensures that Req. 2 is satisfied, but also that a series of R_c -based parameters can be exported.

A LaSC can be systematically denoted by a set of binary tuples in the format $n_h-Si_hj_hk_h$, where n_h is the number of CNS $Si_hj_hk_h$ types in a LaSC; therefore, $CN = \sum n_h$. For example, in the local structure shown in Figure 1a, 2 S555 and 10 S422 can be constructed; thus, it is denoted as (2-555, 10-422). It is easy to prove that a CNS to CNS index is an injective mapping in any LaSC; then, Req. 3 is satisfied.

3. Specific Features of LaSCA

Although a CNS index in LaSCA seems similar to the notation for the pair-wise structures in CNA and the HA-pair, only through LaSCA is the injective mapping of $CNS \leftarrow \rightarrow Sijk$ granted. This advantage enables many rigorous structural analyses; for example, the systematic study of the spatial distribution of complex crystal phases [17] and the critical states of the packing of uniform spheres [21] and their local rotational symmetries [22,23].

In LaSCA, a group of R_c -based parameters can be exported. The value of R_c varies with the local environment of atoms; therefore, the average, the median, the root mean square, and so on, of R_c are also important structure parameters. For example, the temperature dependence of the average of R_c during solidification is useful in identifying the liquid-liquid transition and the critical point where the liquid-solid transition begins [24,25].

Another crucial feature of LaSCA is that the neighborhood between two atoms may be asymmetric. As shown in Figure 2, assume $R_{c-A} > d_{AB} > R_{c-B}$, where d_{AB} is the distance between atoms A and B, and R_{c-A} and R_{c-B} are, respectively, the cutoff distance R_c for atom A and B; then, atom B is one of the neighbors of atom A, but not vice versa. This asymmetric property of neighborhood between atom pairs reflects differences in local packing densities of atoms, providing more structure information about a system. Furthermore, a directed graph, rather than an undirected graph, for a system can be established.

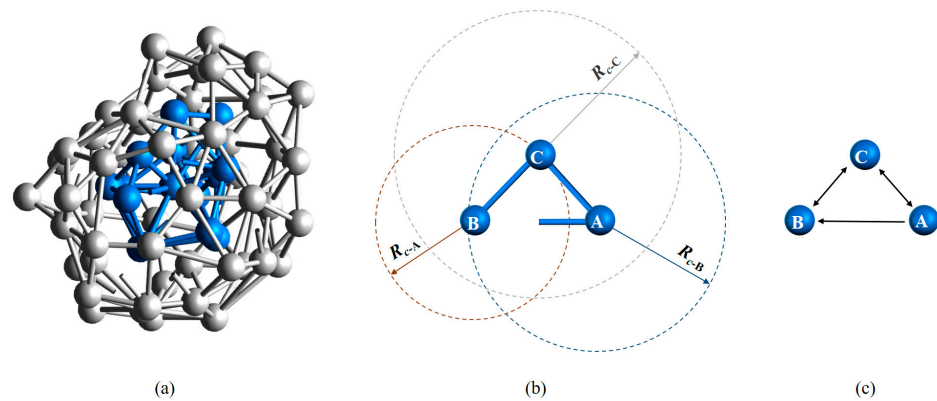


Figure 2. Directed graph representation of interatomic connections. (a) Bonding relationship within a BCC LaSC and that between the neighbor atoms of the BCC LaSC; here, the layer-to-layer bonds are not shown. (b) Bi-directional and one-way edges between atoms. (c) The graphic interpretation of the bonding relationship in (b).

LaSC-Based Visualization Analysis

Without any preset parameters, LaSCA can identify all local structures around every atom in ordered and disordered systems. For example, the structural units of the simple FCC, HCP, and BCC crystals are (12-421), (6-421, 6-422), and (6-444, 8-666), respectively. After the LaSCs around every atom have been identified, more structural parameters, such as coordination number (CN), angle distribution function, and BOO parameters, can also be worked out. The completeness of the characterization of microstructures allows us to define the structural entropy of systems at various hierarchies [26]. Furthermore, a group of structural indexes based on R_c and bond length (such as mean, standard deviation, and root mean square over a system) and their temperature/time dependence in a thermodynamics process are very useful in identifying phase transitions, critical points, and so on [25]. These structural indexes cannot be provided using other methods.

For complex systems, such as the solid-liquid coexistence state during crystallization or the polycrystalline coexistence system, the spatial distribution characteristics of various atoms are extremely important. However, it is very difficult to describe such characteristics using numerical methods; thus, visualization is particularly important at this time.

Focusing on structure analysis (and not only displaying function), a LaSC-based program is developed, also called LaSCA here. Besides identifying local structures (short-range order) around each atom, three primary functions of LaSCA are atom selection, color setting, and size configuration. Atom selection can be based on input features (such as 3D coordination, potential energy, kinetic energy, charge, atom type, and atom ID) and/or export features of LaSCA, including CN, CNS, or LaSC type, as well as LaSC sets (such as atoms with S555). The color and size of atoms can be freely set based on these features. Arbitrary section analysis is supported, and the section can be set in three ways, using the Miller index plus the position of an atom, the midplane of two specified atoms, or the positions of three specified atoms. Additionally, many user-friendly features and advanced structural analysis functions have been designed, some of which are as follows.

- Atom representation automatically switches according to the number of atoms to be displayed, from sphere through icosahedron and tetrahedron to point. This is so that the rendered image is presented as quickly as possible.
- The atom's ID can be displayed and tracked visually. Not only are the ID numbers always facing the user when rotating and transforming, but their size and color can also be configured by users in various ways.
- A variety of ways are available to help users obtain a suitable viewing angle. Users can customize (fix) the rotation axis (OX, OY, OZ, and any axis); when a section is displayed, a "vertical observation" shortcut is provided.

- A set of topologically close-packed (TCP) structures (including Frank–Kasper polyhedrons) can be systematically quantified [27], based on which TCP crystalline regions (such as A15, C15, and σ phase) can be identified [16,17,28,29].
- Long-range ordered structures can be identified with topological criteria. Currently, there are several complex crystals consisting of hexagonally densely packed (HCP) layers, such as double HCP and rhombic crystals.
- Logical OR can be implemented by selecting multiple items after an attribute has been discretized into multiple intervals (items), logical AND is achieved through pipelined operations, and logical NOT is also supported.
- Arbitrary partial PDFs are implemented through ternary mode. With such a function, users can obtain a partial PDF of any type of atom pairs, including element pairs in multi-component alloys and structure-based pairs (FCC, HCP, and BCC atoms) in a complex system [25,30].

4. Case Study

4.1. Long-Range Ordered Structure

It is very difficult to identify long-range ordered structures (composed of at least two types of LaSCs meeting certain spatial distribution characteristics) using numerical calculation. LaSCA has made some useful attempts recently. As shown in Figure 3a, in the double hexagonal close-packed (DHCP) crystal, the repeating unit consists of four HCP layers, where each atom has six neighbors arranged in equilateral triangles, with the ACAB... sequence. Figure 3b presents the distribution of FCC and HCP atoms within a part of a shocked bulk yttrium initialized as an HCP single crystal [31], where atoms are represented by grey points. When the icosahedron is employed to represent atoms that are color-coded by LaSC types, we arrive at Figure 3c. Subsequently, the DHCP long-range ordered structure analysis is performed and DHCP atoms are plotted in Figure 3d, where the long-range periodicity is evident. Currently, the close-packed Rhombohedral (Sm-type) crystal structure can also be identified; its repeating unit is composed of a sequence of nine HCP layers of ABCBCACAB.

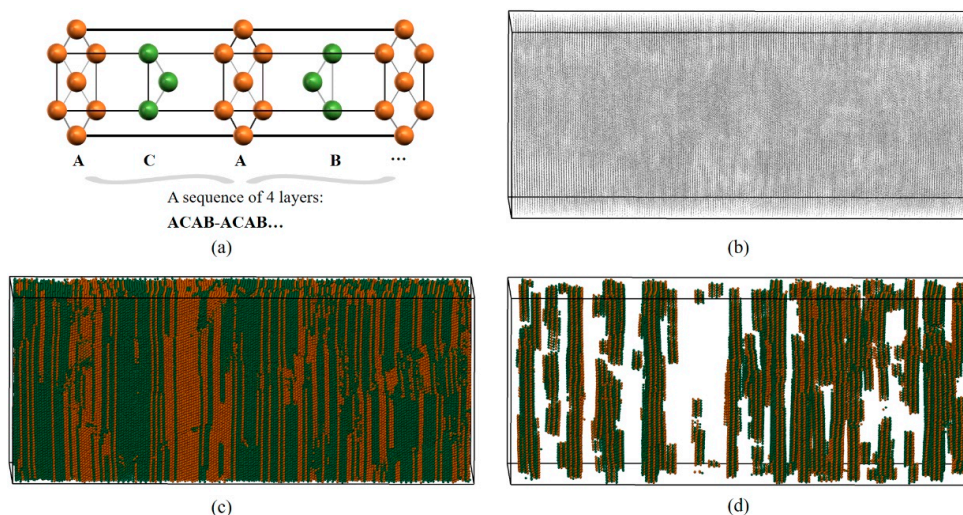


Figure 3. Schematic diagram of DHCP long-range structure analysis of LaSCA. (a) Structural feature of the DHCP crystal. (b) The FCC and HCP atoms represented by grey points. (c) The type-colored FCC and HCP atoms represented by icosahedrons. (d) The DHCP atoms in this system.

4.2. Visual Analysis of Complex Crystal

Based on the LaSC, we defined a set of local structures, the topologically close-packed (TCP) LaSCs that are characterized as $(n_4\text{-S444}, n_5\text{-S555}, n_6\text{-S666})$ with $n_5 > 0$ [27]. According to Euler's Theorem, it is easy to prove that $2 \times n_4 + n_5 = 12$; therefore, the TCP LaSC can be expressed in the more compact format "Ln", where "L" denotes the number of n_4 , ranging

from 0 to 5, with Z, A, B, C, D, and E, respectively, and “ n ” is the coordination number of the central atom ($n = n_4 + n_5 + n_6$). For example, (1-444, 10-555, 2-666) is A13.

The simple FCC, HCP, and BCC crystals are composed of only one type of atom, FCC (12-421), HCP (6-421, 6-422), and BCC (6-444, 8-666) atoms, respectively. However, most of the complex crystals include several types of LaSCs [28]; moreover, the crystal type depends not only on the number ratio of different types of LaSCs, but also on their spatial distribution. In such cases, visual analysis is very useful. Here, a 1200-atom $\text{Fe}_{70}\text{Cu}_{15}\text{Ni}_{15}$ nanoparticle obtained through the rapid cooling of a nanodroplet with MD simulation is chosen to elucidate the visual analysis process, with the key steps shown in Figure 4.

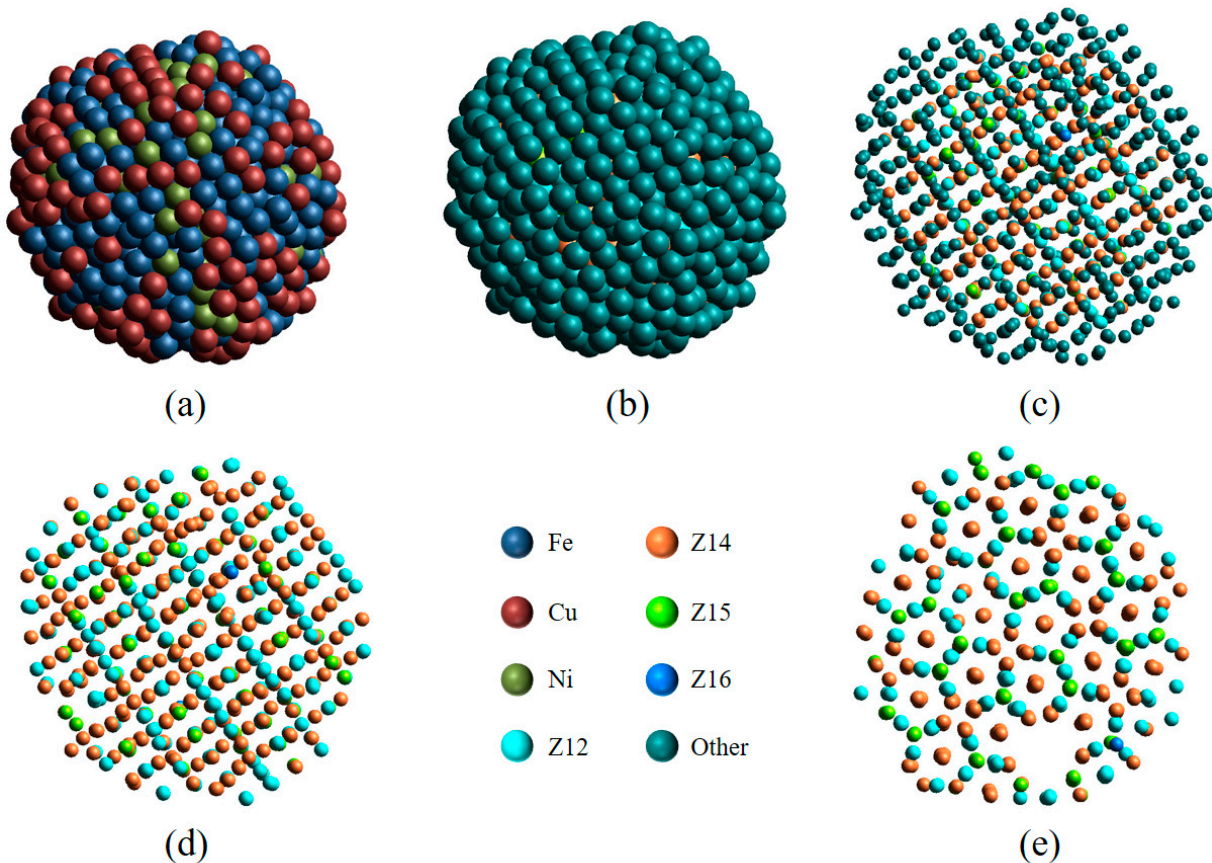


Figure 4. Structural analysis of a $\text{Fe}_{70}\text{Cu}_{15}\text{Ni}_{15}$ nanoparticle. The 3D view is color-coded by element type (a) or by LaSC type (b–e). The radius of atoms in (b,e) is double that of atoms in (c,d). (d,e) Only four TCP (Z12, Z14, Z15, and Z16) atoms retained.

As can be seen in Figure 4a, it looks like an amorphous particle. After the LaSC around each atom has been identified, the atoms are colored by LaSC type (see Figure 4b), where, except for four TCP atoms (Z12, Z14, Z15, and Z16), other atoms are unified in dark green. When the atomic radius is reduced by 60%, their distribution has a clear spatial periodicity (Figure 4c). Then, only four TCP atoms are retained in Figure 4d; the periodicity of the atomic distribution becomes clearer, and the complex spatial feature is obvious. Observed from a different angle, Figure 4e provides another spatial projection (with defects), different from that in Figure 4d. These different projections reveal the structural complexity of this nanoparticle, which is identified as the σ -phase crystal by calculating the number ratio of Z12, Z14, and Z15 atoms [28,29]. With the help of the visual analysis provided by LaSCA and by keeping crystallography expertise in mind, the structural units of other, more complex crystals can also be identified [17].

4.3. Partial PDF Analysis of Multi-Component Alloys

A 5000-atom $\text{Ni}_{70}\text{Ag}_{30}$ nanoparticle is taken to illustrate the function of the partial PDF (pPDF) curves exported by LaSCA. After all the LaSCs are identified, all atoms are grouped according to the LaSC type (see Figure 5a), where tDH (truncated decahedron), FCC, and HCP atoms are considered as group A (1016 atoms), Z12 and Z16 atoms as group B (1621 atoms), and all other atoms as group C (2363 atoms, not shown in Figure 5a), for more details please see the Supplementary video S1: video for constructing Figure 5a. Then, six pPDF curves of the ternary system are exported, where, in order to clarify the contribution of each type of pairs to the total PDF, the summation normalization is conducted [32], i.e., $\sum g_{\alpha\beta}(r) = g_{\text{total}}(r)$.

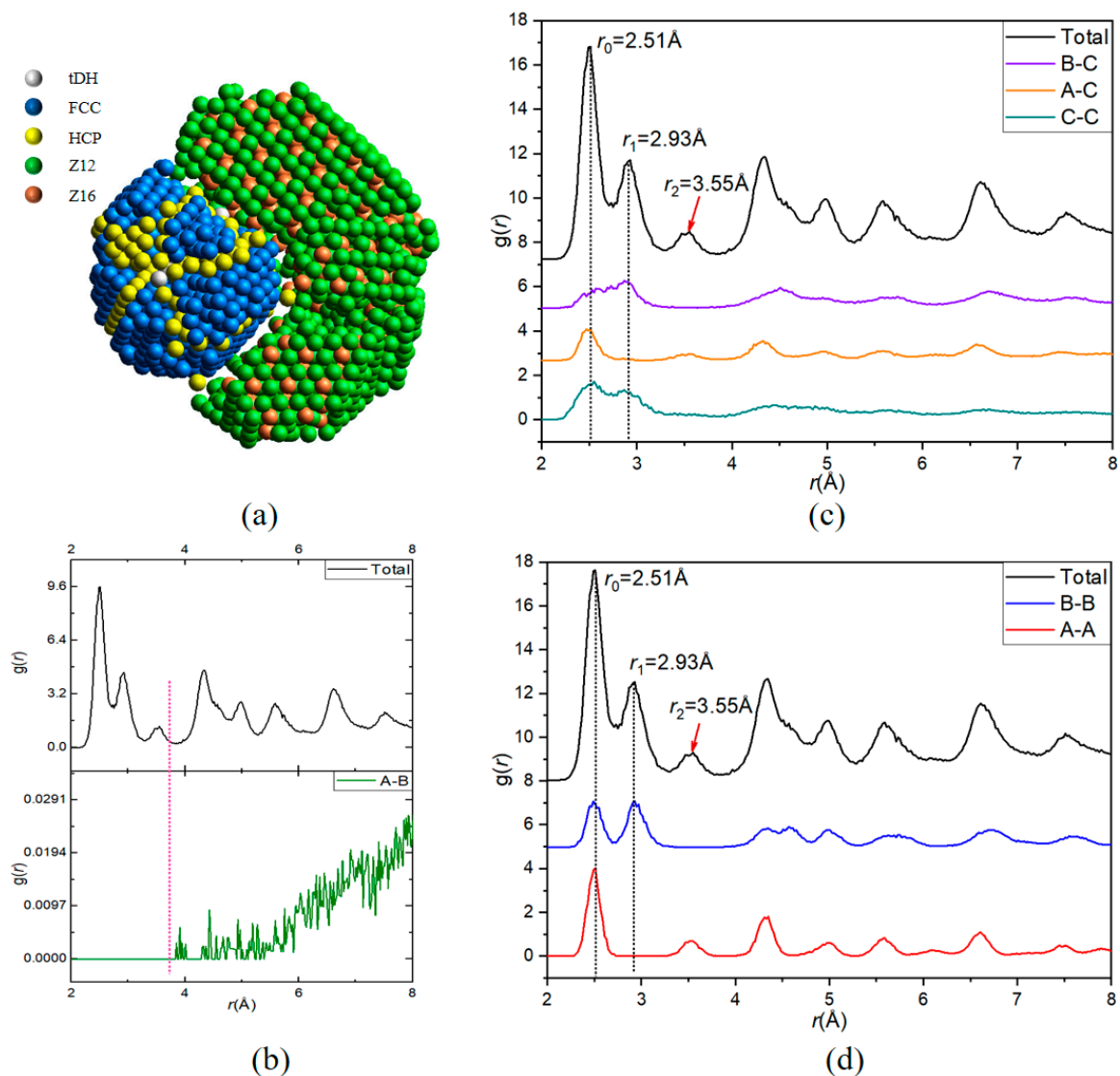


Figure 5. Illustration of partial PDF curves based on a ternary mode with a $\text{Ni}_{70}\text{Ag}_{30}$ nanoparticle. (a) The 3D view for FCC, HCP, tDH, Z12, and Z16 atoms color-coded by LaSC type. (b–d) The correspondence between the total and six partial PDF curves, grouped by the magnitude of curves.

Among six pPDF curves, only the $g_{\text{A-B}}(r)$ (Figure 5b) does not contribute to the first three peaks on the total PDF (see Figure 5a), consistent with the fact that atoms in group A are far away from those in group B. In fact, A atoms comprise a five-fold symmetrical FCC crystalline region, while B atoms comprise a TCP complex crystalline region, and there are wide dislocations (composed of C atoms) between the two crystalline regions.

Zero is the height of both the $g_{A-C}(r)$ (Figure 5c) and the $g_{A-A}(r)$ (Figure 5d) at the position of the second peak on the total PDF; thus, A atoms (belonging to the five-fold symmetrical FCC crystalline region) do not contribute to the second peak on the total PDF, because $g_{A-B}(r)$ is also zero at this position (Figure 5a). In other words, the peak at $r = 1.167 r_0$ ($r_0 = 2.51 \text{ \AA}$ is for the position of the first peak) is caused by TCP structures and the other structures (represented by C atoms). By contrast, only $g_{A-A}(r)$ contributes to the third peak at $r = 1.414 r_0$ on the total PDF (Figure 5d). C atoms have TCP characteristics because $g_{C-C}(r)$ and $g_{B-C}(r)$ contribute to both the first and second peaks, but not to the third peak on the total PDF, whereas $g_{A-C}(r)$ only contributes to the first peak (also slightly to the third peak). Therefore, in combination with the visualization analysis, the pPDF curves can facilitate a better understanding of complex structures.

5. Discussion

With MFC, this tool has been developed using C++ by Zean Tian since August 2005; the binary executable file of LaSCA is now less than 600 M in size, and it is currently only available for Windows operation systems (WIN 7/10), with less than 30 M memory when no data are loaded. It is a parallel version with OpenMP library, to construct parallel identification of the LaSCs around all atoms on the CPU level, and with OpenGL library, to render atoms accelerated by GPU (if available).

Physical correctness, objective identification, and injective representation make LaSCA particularly useful for complex systems, where the height of the first valley on the PDF curve of the system is more than zero and/or the primary local structures include atoms beyond the nearest neighbors (such as the BCC crystal). As shown in Figure 5a, the value of R_c for Z12 and Z16 atoms is about 3.6 \AA , while for HCP and FCC atoms, an R_c less than 2.6 \AA is enough. In other words, neither 3.6 \AA nor 2.6 \AA can be used to identify all types of LaSCs in this nanoparticle. However, for LaSCA, this difficulty does not exist, due to its parameter-free basic properties.

Composed of 12–15 atoms, TCP structures are ubiquitous in nanoparticles, superalloys, high-entropy alloys, and alloys under high-pressure conditions. However, it is difficult to give a strict geometric definition for them, due to their topological properties; thus, numerical identification from simulation samples is difficult. For LaSCA with inherent topological criteria, this problem is straightforwardly solved without any extra effort, as shown in Figures 4 and 5a.

Even though the local structures composed of a complex crystal have been identified, it is still very difficult and computationally costly to recognize such long-range ordered regions, because it is almost impossible to obtain a perfect complex crystal through simulation. LaSCA, which retains the geometric characteristics of the local structure, opens up an available path for the recognition of such crystals based on their topological characteristics, such as the recognition of DHCP atoms in a complex system.

Importantly, clarification of three essential requirements for general structural analysis will guide the development of structural analysis methods; structural indexes based on the LaSCs, such as the structural entropy of a system at various hierarchies and the R_c -based parameters, are key contributions to material science, especially in the field of theoretical research.

In future, AI technology will be introduced for identifying complex structures whose units are composed of tens to hundreds of atoms, such as C15 phase, with a 24-atom unit, and β -Ta, with a 30-atom unit. As a general tool, it will also offer certain additional features, such as the plotting of charge densities and ELFs.

Supplementary Materials: The following supporting information can be downloaded at: <https://www.mdpi.com/article/10.3390/met13020415/s1>, Video S1: video for constructing Figure 5a.

Author Contributions: Conceptualization, Z.T.; methodology, Z.T.; software, Z.T., Z.Z., X.J. and F.W. (Feng Wei); validation, F.W. (Fan Wu); formal analysis, Z.T.; investigation, Z.Z., F.W. (Feng Wei) and S.P.; resources, F.W. (Fan Wu); data curation, Z.T. and X.J.; writing—original draft preparation, Z.Z.; writing—review and editing, Z.T., Z.Z., S.P. and X.J.; visualization, Z.T.; supervision, Z.T. and F.W. (Fan Wu); project administration, Z.T. and Z.Z.; funding acquisition, Z.T. All authors have read and agreed to the published version of the manuscript.

Funding: This research was funded by [National Key R&D Program of China] grant number [2021YFB0300102], [National Natural Science Foundation of China] grant number [U1612442] and [51661005], [Natural Science Foundation of Hunan province] grant number [2022JJ30166], [GHfund A] grant number [2022020119853].

Data Availability Statement: Contact tianzean@hnu.edu.cn via email to obtain the binary executable file of LaSCA. The user manual, where detailed information of LaSCA is provided, can also be obtained via the above email address.

Acknowledgments: Authors acknowledge the financial support of the National Key R&D Program of China (Grant No. 2021YFB0300102), the National Natural Science Foundation of China (Grant Nos. U1612442 and 51661005), and the Natural Science Foundation of Hunan province (Grant No. 2022JJ30166). Research was also supported by the GHfund A (2022020119853).

Conflicts of Interest: The authors declare no conflict of interest. The funders had no role in the design of the study; in the collection, analyses, or interpretation of data; in the writing of the manuscript; or in the decision to publish the results.

References

1. Juhás, P.; Cherba, D.M.; Duxbury, P.M.; Punch, W.F.; Billinge, S.J.L. Ab initio determination of solid-state nanostructure. *Nature* **2006**, *440*, 655–658. [[CrossRef](#)] [[PubMed](#)]
2. Streitz, F.H.; Glosli, J.N.; Patel, M.V. Beyond Finite-Size Scaling in Solidification Simulations. *Phys. Rev. Lett.* **2006**, *96*, 225701. [[CrossRef](#)] [[PubMed](#)]
3. Cliffe, M.J.; Dove, M.T.; Drabold, D.A.; Goodwin, A.L. Structure Determination of Disordered Materials from Diffraction Data. *Phys. Rev. Lett.* **2010**, *104*, 125501. [[CrossRef](#)] [[PubMed](#)]
4. Faken, D.; Jónsson, H. Systematic analysis of local atomic structure combined with 3D computer graphics. *Comput. Mater. Sci.* **1994**, *2*, 279–286. [[CrossRef](#)]
5. Qi, D.W.; Wang, S. Icosahedral order and defects in metallic liquids and glasses. *Phys. Rev. B* **1991**, *44*, 884–887. [[CrossRef](#)]
6. Honeycutt, J.D.; Andersen, H.C. Molecular dynamics study of melting and freezing of small Lennard-Jones clusters. *J. Phys. Chem.* **1987**, *91*, 4950–4963. [[CrossRef](#)]
7. Aste, T. Variations around disordered close packing. *J. Phys. Condens. Matter* **2005**, *17*, S2361–S2390. [[CrossRef](#)]
8. Jonsson, H.; Andersen, H.C. Icosahedral Ordering in the Lennard-Jones Liquid and Glass. *Phys. Rev. Lett.* **1988**, *60*, 4. [[CrossRef](#)]
9. Polak, W.Z. Efficiency in identification of internal structure in simulated monoatomic clusters: Comparison between common neighbor analysis and coordination polyhedron method. *Comput. Mater. Sci.* **2022**, *201*, 110882. [[CrossRef](#)]
10. Tuceryan, M.; Jain, A.K. Texture Segmentation Using Voronoi Polygons. *IEEE Trans. Pattern Anal. Mach. Intell.* **1990**, *12*, 211–216. [[CrossRef](#)]
11. Jones, T.R.; Carpenter, A.; Golland, P. Voronoi-Based Segmentation of Cells on Image Manifolds. In *Computer Vision for Biomedical Image Applications*; Liu, Y., Jiang, T., Zhang, C., Eds.; Lecture Notes in Computer Science; Springer: Berlin, Heidelberg, 2005; Volume 3765, pp. 535–543, ISBN 978-3-540-29411-5.
12. Tian, Z.A.; Liu, R.S.; Dong, K.J.; Yu, A.B. A new method for analyzing the local structures of disordered systems. *EPL* **2011**, *96*, 36001. [[CrossRef](#)]
13. Wang, S.Y.; Tian, Z.A.; Dong, K.J.; Xie, Q. Inconsistency of neighborhood based on Voronoi tessellation and Euclidean distance. *J. Alloy. Compd.* **2021**, *854*, 156983. [[CrossRef](#)]
14. Li, H.L.; Karina, A.; Ladd-Parada, M.; Späh, A.; Perakis, F.; Benmore, C.; Amann-Winkel, K. Long-Range Structures of Amorphous Solid Water. *J. Phys. Chem. B* **2021**, *125*, 13320–13328. [[CrossRef](#)]
15. Zhou, L.L. Pressure effect on structure and properties of rapidly cooled Mg₇₀Zn₃₀ alloy. *J. Mater. Sci.* **2021**, *56*, 4420–4432. [[CrossRef](#)]
16. Mo, Y.F. The short-range order in liquid and A15 crystal of zirconium. *J. Non-Crystalline Solids* **2019**, *513*, 111–119. [[CrossRef](#)]
17. Jiang, M.X.; Tian, Z.A.; Xie, Q.; Gao, T.H.; Liang, Y.C.; Chen, Q. Numerical recognition of C15 unit in rapid solidification Ni₇₀Ag₃₀ nanoparticles. *Acta Phys. Sin.* **2022**, *71*, 176402. [[CrossRef](#)]
18. Pennington, W.T. DIAMOND— Visual Crystal Structure Information System. *J. Appl. Crystallogr.* **1999**, *32*, 1028–1029. [[CrossRef](#)]
19. Mendelsohn, L.D. ChemDraw 8 Ultra, Windows and Macintosh Versions. *J. Chem. Inf. Comput. Sci.* **2004**, *44*, 2225–2226. [[CrossRef](#)]

20. Stukowski, A. Visualization and analysis of atomistic simulation data with OVITO—the Open Visualization Tool. *Model. Simul. Mater. Sci. Eng.* **2010**, *18*, 015012. [[CrossRef](#)]
21. Tian, Z.A.; Dong, K.J.; Yu, A.B. Structural evolution in the packing of uniform spheres. *Phys. Rev. E* **2014**, *89*, 032202. [[CrossRef](#)]
22. Tian, Z.A.; Dong, K.J.; Yu, A.B. Structural evolution in the crystallization of rapid cooling silver melt. *Ann. Phys.* **2015**, *354*, 499–510. [[CrossRef](#)]
23. Radziuk, D.; Möhwald, H. Ultrasonically treated liquid interfaces for progress in cleaning and separation processes. *Phys. Chem. Chem. Phys.* **2016**, *18*, 21–46. [[CrossRef](#)] [[PubMed](#)]
24. Luo, Y.C.; Tian, Z.A.; Zheng, Q.; Hu, L.; Dong, K.J. Crystallization insights revealed by simulation solidification study of Fe₆₃Ni₃₃Co₄ alloy melt at subcritical cooling rate. *J. Non-Cryst. Solids* **2022**, *586*, 121557. [[CrossRef](#)]
25. Hu, L. The role of TCP structures in glass formation of Ni₅₀Ag₅₀ alloys. *J. Alloy. Compd.* **2022**, *897*, 162743. [[CrossRef](#)]
26. Li, J.J.; Tian, Z.A.; Xie, Q.; Xiong, S.X. Component effect on microstructure of rapidly cooled FeCuNi alloys. *Chem. Phys. Lett.* **2020**, *753*, 137630. [[CrossRef](#)]
27. Frank, F.C.; Kasper, J.S. Complex alloy structures regarded as sphere packings. II. Analysis and classification of representative structures. *Acta Cryst.* **1959**, *12*, 483–499. [[CrossRef](#)]
28. Wu, Z.Z.; Mo, Y.F.; Lang, L.; Yu, A.B.; Xie, Q.; Liu, R.S.; Tian, Z.A. Topologically close-packed characteristic of amorphous tantalum. *Phys. Chem. Chem. Phys.* **2018**, *20*, 28088–28104. [[CrossRef](#)]
29. Li, X.; Tian, Z.A.; Xie, Q.; Dong, K.J. The topologically close-packed Fe₇₀Cu₁₅Ni₁₅ nanoparticles—A simulation study. *Vacuum* **2021**, *193*, 110523. [[CrossRef](#)]
30. Li, J.J.; Tian, Z.A. Structural Origin of the Second Peak Split of FeCuNi Metallic Glass. *Low Temp. Phys. Lett.* **2020**, *42*, 81–89. [[CrossRef](#)]
31. Liu, B.B.; Chen, Y.C.; Guo, L.; Li, X.F.; Wang, K.; Deng, H.Q.; Tian, Z.A.; Hu, W.Y.; Xiao, S.F.; Yuan, D.W. Shock-induced phase transition in yttrium between multilayered hexagonal closedpacked structures by atomistic simulations. *Int. J. Mech. Sci.* **2023**, *submitted*.
32. Lang, L.; Deng, H.Q.; Tian, Z.A.; Gao, F.; Hu, W.Y.; Wen, D.D.; Mo, Y.F. The effect of Mo addition on structure and glass forming ability of Ni-Zr alloys. *J. Alloy. Compd.* **2019**, *775*, 1184–1198. [[CrossRef](#)]

Disclaimer/Publisher’s Note: The statements, opinions and data contained in all publications are solely those of the individual author(s) and contributor(s) and not of MDPI and/or the editor(s). MDPI and/or the editor(s) disclaim responsibility for any injury to people or property resulting from any ideas, methods, instructions or products referred to in the content.